

1 **Kinetic Characteristics of Electrochemical Reduction of SiO₂ Granules in Molten CaCl₂**

2

3 Xiao Yang^{a,*}, Kouji Yasuda^{a,b}, Toshiyuki Nohira^{a,*z}, Rika Hagiwara^{a,*}, and Takayuki Homma^{c,*}

4

5 ^a Graduate School of Energy Science, Kyoto University, Yoshida-honmachi, Sakyo-ku, Kyoto

6 606-8501, Japan

7 ^b Environment, Safety and Health Organization, Kyoto University, Yoshida-honmachi, Sakyo-ku,

8 Kyoto 606-8501, Japan

9 ^c Faculty of Science and Engineering, Waseda University, 3-4-1 Okubo, Shinjuku-ku, Tokyo

10 169-8555, Japan

11

12 * Electrochemistry Society Active Member

13 ^z E-mail: nohira@energy.kyoto-u.ac.jp

14

15

16

Abstract

17 The kinetic characteristics of electrochemical reduction of SiO₂ granules in molten CaCl₂ were
18 investigated to develop a new process for producing solar-grade silicon. The reduction rate was
19 evaluated based on the time dependence of the reduction fractions measured from the growth of the
20 reduced Si layer and the weight change of the samples during electrolysis. The samples were
21 prepared by potentiostatic electrolysis of SiO₂ granules in molten CaCl₂ at 1123 K. The results
22 indicated that the reduction was fast at the initial stage of electrolysis, and gradually slowed as the
23 reaction progressed. The apparent current density reached 0.7 A cm⁻² at the initial stage, which was
24 comparable to the commercial Hall-Héroult process for aluminum production.

25

26

27 **Key Words:** Solar-grade Silicon, Silica, Electrolysis, Molten Salt, Kinetics, Current Density

28

29

Introduction

30 The global solar cell market has grown rapidly over the past decade. The annual installation of
31 solar cells in the world reached 28.6 GW in 2012.¹ Crystalline silicon is the most prevalent raw
32 material for solar cells on the market, and Si-based solar cells accounted for 88% of the global
33 production in 2012.² With the expansion of the market, the consumption of solar-grade silicon
34 (SOG-Si; 6N purity) has also climbed dramatically. An average growth of 10–20% per year is
35 estimated for SOG-Si production over the next decade.

36 The Siemens process,³⁻⁵ based on hydrogen reduction and thermal decomposition of
37 trichlorosilane (SiHCl_3), is the most widely used process for SOG-Si production. In spite of the
38 highly reliable product quality, this process has some disadvantages, including low productivity, low
39 reaction efficiency, and high energy consumption. Therefore, a novel, high yielding, inexpensive
40 SOG-Si production process is required.

41 Various SOG-Si production processes have been developed to displace the Siemens process.⁶⁻²⁵
42 Meanwhile, the authors²⁶⁻³³ and other researchers³⁴⁻⁴³ have demonstrated that solid silica (SiO_2) can
43 be directly reduced to solid Si via electrolysis in molten salts. A SiO_2 plate or pellet in contact with a
44 current conductor is electrochemically reduced to Si at the three-phase zone of SiO_2 /molten
45 salt/conductor. The produced O^{2-} ions are transferred to the carbon anode through the melt, and then
46 oxidized to form CO or CO_2 . The authors has proposed a new SOG-Si production process by

47 combining this method with the use of high-purity silica and directional solidification,³² and
48 demonstrated that impurities in the produced Si can be controlled at a low level when high-purity
49 SiO₂ is used as the raw material.⁴⁴

50 Recently, the authors proposed an improved electrochemical process in which SiO₂ granules are
51 directly used as the raw material.⁴⁵ From the viewpoint of industrial application in the future,
52 granules have advantages in cost and quality control over plates or pellets, as well as the suitability
53 for a continuous operation. SiO₂ granules are supplied from the top of the electrolysis cell and are
54 stratified on the cathode placed at the bottom of the cell. The electrochemically reduced Si in molten
55 CaCl₂ is tapped out from the cell bottom as slurry containing molten CaCl₂. The advantage of this
56 process is the compatibility for a semi-continuous operation, which improves the productivity.

57 The kinetics of the direct electrochemical reduction of solid SiO₂ granules is crucial for the scale
58 up of the laboratory experiment for commercial production. Previously, the kinetics was studied
59 based on the current-time curve during electrolysis⁴⁵ and direct observation of the reaction
60 interface.⁴⁶ The overall reduction was clarified to proceed via two different routes: (1) from the SiO₂
61 granules near the conductor to the distant granules along the granule surfaces, and (2) from the
62 surface to the core in each partly reduced granule. Formation of the core (SiO₂)–shell (Si) structure
63 for partly reduced SiO₂ granules indicated that the reduction along the granule surfaces was faster
64 than that from the surface to the core.

65 In the present study, the kinetic characteristics of the electrochemical reduction of SiO₂ granules
66 in molten CaCl₂ at 1123 K were further investigated by the direct measurement of the reaction
67 interfaces and the weight change of the samples during electrolysis. The kinetics was discussed by
68 plotting the time dependence of the reduction fraction. The productivity of the proposed process was
69 evaluated based on the apparent current density calculated from the experimental results.

70

71 **Experimental**

72 An Al₂O₃ crucible (Nikkato Corp., o.d. 90 × i.d. 80 × height 100 mm) charged with 300 g of
73 CaCl₂ (Kojundo Chemical Lab. Co., Ltd., 99%) was set inside a SiO₂ vessel and heated to 1123 K in
74 a dry Ar atmosphere (100 mL min⁻¹) in an electric furnace. Prior to the experiment, CaCl₂ was dried
75 under vacuum at 453 K for 72 h and 773 K for 24 h. The working electrode comprised an Al₂O₃ tube
76 (Nikkato Corp. o.d. 13 × i.d. 9 × height 10 mm) and a Si plate (Nilaco Corp., □15.0 × thickness 0.5
77 mm, n-type, (100) plane, resistivity 0.1–1.0 Ω cm) (Figure 1). A nickel wire (Nilaco Corp., □1.0 mm,
78 99%) used as the current lead was connected to the Si plate by threading into a drilled hole (□1.1
79 mm). Approximately 0.41 g of high-purity SiO₂ granules (Taiheiyo Cement Corp., particle size < 0.1
80 mm) was charged in the Al₂O₃ tube. With this setup, electrical contact to SiO₂ occurs only through
81 the Si plate at the bottom of the Al₂O₃ tube.

Fig. 1

82 A glassy carbon rod (Tokai Carbon Co., Ltd., □5.2 mm) was used as the counter electrode. The

83 reference electrode was a Ag^+/Ag electrode prepared by immersing a silver wire (Nilaco Corp., $\square 1.0$
84 mm, 99%) in a CaCl_2 melt containing 0.5 mol% AgCl (Wako Pure Chemical Co., Ltd., 99.5%) in a
85 mullite tube (Nikkato Corp., o.d. $6 \times$ i.d. $4 \times$ height 450 mm). The potential of this reference
86 electrode was occasionally checked against a Ca^{2+}/Ca dynamic reference electrode, prepared
87 galvanostatically on a Mo wire (Nilaco Corp., $\square 1.0$ mm, 99.95%).³¹ All potentials are given with
88 reference to the Ca^{2+}/Ca potential.

89 After immersing the electrodes in the CaCl_2 melt, the potential of the working electrode was set at
90 0.5 V vs. Ca^{2+}/Ca for the potentiostatic electrolysis for 10 min to 240 min. The working electrode
91 was immediately taken out from the melt after electrolysis and a new one was immersed in for
92 another run. The post-electrolysis working electrode was cut vertically into two halves with a
93 diamond wheel saw (SBT 650, Meiwafofos Co., Ltd.) to observe the cross section and measure the
94 thickness of the reduced layer. The kinetics was evaluated by measuring the weight change of the
95 sample between before and after electrolysis. After electrolysis, the sample was first washed in 1M
96 HCl for 24 h. Here, byproducts like CaSiO_3 , CaO and CaCO_3 react with HCl leaving SiO_2 as the
97 only solid residue. Then, the sample was further washed in distilled water for 48 h, and weighed
98 after drying.

99 Blank electrolysis tests using the working electrodes without charging SiO_2 granules were
100 conducted before and during the experiment. Large and unstable background currents (*ca.* -100 mA)

101 were detected, which were mainly due to the side electrochemical reactions of moisture. Since the
102 area of Si plate contacting only the molten salt was larger than the area contacting SiO₂ granules
103 (See Fig. 1b), it was difficult to precisely evaluate the current corresponding only to the SiO₂
104 reduction.

105

106

Results and Discussion

107 **Growth of Reduced Layer.** —The cross sections of the working electrodes after electrolysis at 0.5
108 V vs. Ca²⁺/Ca for (a) 10 min, (b) 30 min, (c) 60 min, and (d) 120 min in molten CaCl₂ at 1123 K are
109 shown in Figure 2. For each sample, a dark brown layer was observed above the Si plate at the
110 bottom. Formation of crystalline Si in this layer was confirmed by XRD and SEM/EDX in a
111 previous study with a similar experimental setup.⁴⁶

Fig. 2

112 The dark layer, composed of reduced Si, grows from the bottom to the top with the progress of
113 electrolysis. After 120 min of electrolysis, most of the colorless 6.0-mm-thick SiO₂ layer became
114 dark. The top position of unreduced SiO₂ layer did not apparently change after reduction, as seen in
115 Figure 2. This indicates that the granules piled on the Si plate as a whole do not shrink downward
116 during the reduction. In the similar manner as quartz plate,²⁶ the volume decrease from SiO₂ to Si is
117 explained by the formation of porous structure inside the granule. The thicknesses of the dark layer
118 at three different positions for each image in Figure 2 were measured using a ruler. The average

Fig. 3

119 value of the reduced layer is plotted against electrolysis time in Figure 3. The growth rate of the
120 reduced layer gradually decreased with the electrolysis progress.

121

122 **Weight Change during Electrolysis.**— The progress of the electrochemical reduction was
123 investigated by measuring the weight change of the samples. The mass balance before and after

Fig. 4

124 electrolysis is illustrated in Figure 4, where $W_{\text{bef.}}$ and $W_{\text{aft.}}$ are the weights of the samples before and
125 after electrolysis. Here, the dissolution of solid SiO_2 in molten CaCl_2 is not considered. Because the

126 Si atoms remain in the tube during the electrolysis, the weight change occurs by the removal of

Table I

127 oxygen. The weight change after 10–240 min of electrolysis are listed in Table I and plotted against
128 electrolysis time in Figure 5. In accordance with the growth rate of the reduced layer, the rate of the

Fig. 5

129 weight change is large at the initial stage of electrolysis compared with the later stage.

130

131 **Reduction Fraction during Electrolysis.**— The reduction fraction was evaluated by two methods.

132 From the perspective of the growth of the reduced layer, the apparent reduction fraction ($F_{\text{app.}}$) is

133 defined as

134
$$F_{\text{app.}} = \frac{\delta_{\text{red.}}}{\delta_{\text{ini.}}} \times 100\% \quad (1)$$

135 where $\delta_{\text{red.}}$ and $\delta_{\text{ini.}}$ are the thicknesses of the reduced layer and the initial SiO_2 layer (Figure 2).

136 Secondly, the actual reduction fraction ($F_{\text{act.}}$) is calculated from the weight change of the samples

137 during electrolysis by

$$138 \quad F_{\text{act}} = \frac{(W_{\text{bef.}} - W_{\text{aft.}}) \cdot \frac{M_{\text{SiO}_2}}{2M_{\text{O}}}}{W_{\text{bef.}}} \times 100\% \quad (2)$$

139 where M_{SiO_2} and M_{O} are the molar weights of SiO_2 and O, respectively.

140 The apparent and actual reduction fractions are listed in Table II. The time dependences of the

Table II

141 reduction fractions are compared in Figure 6. The apparent reduction fraction was larger than the

Fig. 6

142 actual value. The difference is due to the formation of the core (SiO_2)–shell (Si) structure for the

143 partly reduced SiO_2 granules (Figure 7).⁴⁶ The SiO_2 granules in the reduced layer were not

Fig. 7

144 completely reduced to Si.

145 $F_{\text{app.}}$ and $F_{\text{act.}}$ rapidly increased at the initial stage of electrolysis as compared with the later stage.

146 This tendency indicates that the reduction gradually slows with the progress of electrolysis, and two

147 potential explanations can be considered. First, contact resistance exists between formed Si particles,

148 resulting in a voltage drop. With the progress of electrolysis, the reduction front gradually moves

149 away from the start point (Si plate) leading to a large voltage loss by contact resistance. The

150 reduction rate has been reported to decrease at more positive potentials.^{26,27,29} Because the contact

151 resistance would be primarily generated at the surface of Si granules, this effect plays an important

152 role on the behavior of $F_{\text{app.}}$. Moreover, the diffusion of O^{2-} ions in CaCl_2 inside the granules

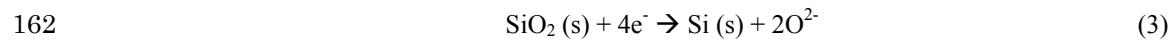
153 becomes important when the reduction proceeds. For the reduction along the granule surface, the

154 formed O^{2-} ions immediately diffuse into the bulk CaCl_2 . For the reduction inside, the formed O^{2-}

155 ions must diffuse through the crevice of the Si shell. As explained in the previous study,^{45,46} the O²⁻
 156 ions accumulate in the CaCl₂ in the crevice, leading to an increased viscosity of CaCl₂ and decreased
 157 diffusion coefficient of the O²⁻ ions. Consequently, the reduction rate decelerates with the progress of
 158 electrolysis, which is predominantly responsible for the behavior of F_{act} .

159

160 **Apparent Current Density.**— The current density, an important kinetic index, is evaluated from
 161 the weight change of the samples. The electrochemical reduction of SiO₂ is written as



163 The quantity of cathodic electric charge (Q) used for the reduction of SiO₂ can be calculated by

$$164 \quad Q = \frac{W_{\text{bef.}} - W_{\text{aft.}}}{2M_{\text{O}}} \times 4e \cdot N_{\text{A}} \quad (4)$$

165 where e is the elementary charge of an electron ($e \approx 1.6 \times 10^{-19}$ C), and N_{A} is Avogadro's constant
 166 ($N_{\text{A}} \approx 6.02 \times 10^{23} \text{ mol}^{-1}$). The apparent current density (J) based on the geometric area of the bottom

167 conductor (Si plate in Figure 1) can be obtained by

$$168 \quad J = \frac{Q}{A \cdot t} = \frac{Q}{\pi \cdot \frac{d^2}{4} \cdot t} \quad (5)$$

169 where A is the valid geometrical area of the Si plate, d is the inner diameter of the Al₂O₃ tube ($d =$
 170 0.9 cm), and t is the electrolysis time. In the present study, cathodic charge and current are taken as
 171 positive values.

172 The calculated apparent current density is listed in Table II, and its time dependence is shown in

173 Figure 8. The current density was as large as 0.7 A cm^{-2} at the initial stage, ca. 20 min, and
174 gradually decreased with the progress of electrolysis. This value is comparable to the current
175 density of the commercial Hall-Héroult process for aluminum production.⁴⁷ This result indicates
176 that the direct electrochemical reduction of SiO_2 in molten CaCl_2 has the potential of being a highly
177 productive silicon production process.

178

179

Conclusions

180 The kinetic characteristics of the electrochemical reduction of SiO_2 granules in molten CaCl_2 at
181 1123 K were investigated by direct observation of cross-sectioned samples and weight change of
182 samples during electrolysis.. The results indicated that the reduction was fast at the initial stage of
183 electrolysis and gradually slowed as the electrolysis progressed. The apparent current density
184 reached 0.7 A cm^{-2} at the initial stage of electrolysis. The direct electrochemical reduction of SiO_2 in
185 molten CaCl_2 has the potential of being a silicon production process with high productivity
186 comparable to the commercial Hall-Héroult process.

187

188

Acknowledgements

189 This study was partly supported by JST-CREST and Grants-in-Aid for Scientific Research A from
190 the Japan Society for the Promotion of Science (JSPS). We thank Taiheiyo Cement Corporation for
191 providing high purity SiO₂ granules.

192

193

References

- 194 1. *Global market outlook for photovoltaics 2013-2017*, European Photovoltaic Industry
195 Association, Brussels (2013).
- 196 2. *Rare Metal News*, Arumu Publishing Co., Tokyo (2013).
- 197 3. H. Schweickert, K. Reuschel, and H. Gutsche, U.S. patent 3,011,877 (1961).
- 198 4. H. Gutsche, U.S. patent 3,042,494 (1962).
- 199 5. H. Oda, *Kogyo Zairyo*, **55**, 30 (2007).
- 200 6. H. S. N. Setty, C. L. Yaws, B. R. Martin and D. J. Wangler, U.S. Patent 3,963,838 (1976).
- 201 7. S. Wakamatsu and H. Oda, PCT International Patent, WO2001/085613 (2001).
- 202 8. W. Dieter, European Patent 1,544,167 (2005).
- 203 9. K. Yasuda, K. Morita, T. H. Okabe, *Energy Technology*, **2**, 141 (2014).
- 204 10. S. Honda, M. Yasueda, S. Hayashida and M. Yamaguchi, Japanese Patent Application,
205 H19-145663 (2007).
- 206 11. K. Saegusa and T. Yamabayashi, PCT International patent WO2007/001093 (2007).
- 207 12. K. Yasuda and T. H. Okabe, *JOM*, **62**, 94 (2010).
- 208 13. K. Yasuda, K. Saegusa, and T. H. Okabe, *Metall. Mater. Trans. B*, **42**, 37 (2011).
- 209 14. K. Suzuki, T. Kumagai and N. Sano, *ISIJ Int.*, **32**, 630 (1992).
- 210 15. T. Ikeda and M. Maeda, *ISIJ Int.*, **32**, 635 (1992).

- 211 16. N. Yuge, H. Baba and F. Aratani, U.S. Patent 5,182,091 (1993) .
- 212 17. Y. Sakaguchi, M. Ishizaki, T. Kawahara, M. Fukai, M. Yoshiyagawa and F. Aratani, *ISIJ Int.*, **32**,
- 213 643 (1992).
- 214 18. M. D. Johnston, L. T. Khajavi, M. Li, S. Sokhanvaran and M. Barati, *JOM*, **64**, 935 (2012).
- 215 19. T. Yoshikawa and K. Morita, *JOM*, **64**, 946 (2012).
- 216 20. J. Sanchez, J. Barona, E. Conejero, M. Canle, X. Rel, P. Garcia, and M. Martinez, U.S. Patent
- 217 US008168123B2 (2012).
- 218 21. B. G. Gribov and K. V. Zinov'ev, *Inorg. Mater.*, **39**, 653 (2003).
- 219 22. D. Elwell and R. S. Feigelson, *Sol. Energy Mater.*, **6**, 123 (1982).
- 220 23. D. Elwell and G. M. Rao, *J. Appl. Electrochem.*, **18**, 15 (1988).
- 221 24. J. Olson and K. Carleton, *J. Electrochem. Soc.*, **128**, 2698 (1981).
- 222 25. J. Cai, X. Luo, G. M. Haarberg, O. E. Kongstein, and S. Wang, *J. Electrochem. Soc.*, **159**, D155
- 223 (2012).
- 224 26. T. Nohira, K. Yasuda, and Y. Ito, *Nat. Mater.*, **2**, 397 (2003).
- 225 27. K. Yasuda, T. Nohira, K. Amezawa, Y. H. Ogata, and Y. Ito, *J. Electrochem. Soc.*, **152**, D69
- 226 (2005).
- 227 28. K. Yasuda, T. Nohira, Y. H. Ogata, and Y. Ito, *Electrochim. Acta*, **51**, 561 (2005).
- 228 29. K. Yasuda, T. Nohira, and Y. Ito, *J. Phys. Chem. Solids*, **66**, 443 (2005).

- 229 30. K. Yasuda, T. Nohira, Y. H. Ogata, and Y. Ito, *J. Electrochem. Soc.*, **152**, D208 (2005).
- 230 31. K. Yasuda, T. Nohira, R. Hagiwara, and Y. H. Ogata, *J. Electrochem. Soc.*, **154**, E95 (2007).
- 231 32. K. Yasuda, T. Nohira, R. Hagiwara, and Y. H. Ogata, *Electrochim. Acta.*, **53**, 106 (2007).
- 232 33. K. Yasuda, T. Nohira, K. Takahashi, R. Hagiwara, and Y. H. Ogata, *J. Electrochem. Soc.*, **152**,
- 233 D232 (2005).
- 234 34. W. Xiao, X. Wang, H. Yin, H. Zhu, X. Mao, and D. Wang, *RSC Advances*, **2**, 7588 (2012).
- 235 35. X. Jin, P. Gao, D. Wang, X. Hu, and G. Z. Chen, *Angew. Chem.*, **116**, 751 (2004).
- 236 36. P. C. Pistorius and D. J. Fray, *J. S. Afr. Inst. Min. Metall.*, **106**, 31 (2006).
- 237 37. W. Xiao, X. Jin, Y. Deng, D. Wang, X. Hu, and G. Z. Chen, *ChemPhysChem.*, **7**, 1750 (2006).
- 238 38. W. Xiao, X. Jin, Y. Deng, D. Wang, X. Hu, and G. Z. Chen, *J. Electroanal. Chem.*, **639**, 130
- 239 (2010).
- 240 39. S. K. Cho, F. F. Fan, and A. J. Bard, *Electrochim. Acta*, **65**, 57 (2012).
- 241 40. E. Juzeliunas, A. Cox, and D. J. Fray, *Electrochem. Comm.*, **12**, 1270 (2010).
- 242 41. E. Ergül, İ. Karakaya, and M. Erdoğan, *J. Alloy. Compd.*, **509**, 89 (2011).
- 243 42. Y. Jiang, J. Xu, X. Guan, U.B. Pal, and S.N. Basu, *MRS Proceedings*, **1493**, 231(2013).
- 244 43. T. Oishi, M. Watanabe, K. Koyama, M. Tanaka, and K. Saegusa, *J. Electrochem. Soc.*, **158**,
- 245 E93(2011).
- 246 44. K. Yasuda, T. Nohira, K. Kobayashi, N. Kani, T. Tsuda, and R. Hagiwara, *Energy Technology*, **1**,

- 247 245 (2013).
- 248 45. T. Toba, K. Yasuda, T. Nohira, X. Yang, R. Hagiwara, K. Ichitsubo, K. Masuda, and T. Homma,
249 *Electrochem.*, **81**, 559 (2013).
- 250 46. X. Yang, K. Yasuda, T. Nohira, R. Hagiwara, and T. Homma, *Metall. Mater. Trans. B*, in press
251 (2014). doi:10.1007/s11663-014-0056-5
- 252 47. J. W. Evans, *JOM*, **59**, 30 (2007).

253 **Caption List**

254 Table I. Weight change of samples during electrolysis at 0.5 V vs. Ca^{2+}/Ca for 10-240 min in molten
255 CaCl_2 at 1123 K.

256 Table II. Apparent reduction fraction (F_{app}), actual reduction fraction (F_{act}), and apparent current
257 density of direct electrochemical reduction of SiO_2 granules by electrolysis at 0.5 V vs.
258 Ca^{2+}/Ca for 10-240 min in molten CaCl_2 at 1123 K.

259

260 Figure 1. (a) Schematic illustration and (b) photograph of the working electrode.

261 Figure 2. Photographs of the cross sections of working electrodes after electrolysis at 0.5 V vs.
262 Ca^{2+}/Ca for 10-120 min in molten CaCl_2 at 1123 K.

263 Figure 3. Time dependence of the thickness of the reduced layer of electrochemical reduction of
264 SiO_2 granules by electrolysis at 0.5 V vs. Ca^{2+}/Ca for 10-120 min in molten CaCl_2 at 1123 K.

265 Figure 4. Schematic illustration of mass balance during electrolysis.

266 Figure 5. Time dependence of weight change of samples during electrolysis at 0.5 V vs. Ca^{2+}/Ca for
267 10-240 min in molten CaCl_2 at 1123 K.

268 Figure 6. Time dependences of reduction fractions of electrochemical reduction of SiO_2 granules by
269 electrolysis at 0.5 V vs. Ca^{2+}/Ca for 10-240 min in molten CaCl_2 at 1123 K.

270 Figure 7. Schematic illustrations of the (a) cross section of the working electrode half way through
271 electrolysis and (b) core (SiO_2)-shell (Si) structure for partly reduced SiO_2 granules.

272 Figure 8. Time dependence of the apparent current density of electrochemical reduction of SiO_2
273 granules by electrolysis at 0.5 V vs. Ca^{2+}/Ca for 10-240 min in molten CaCl_2 at 1123 K.

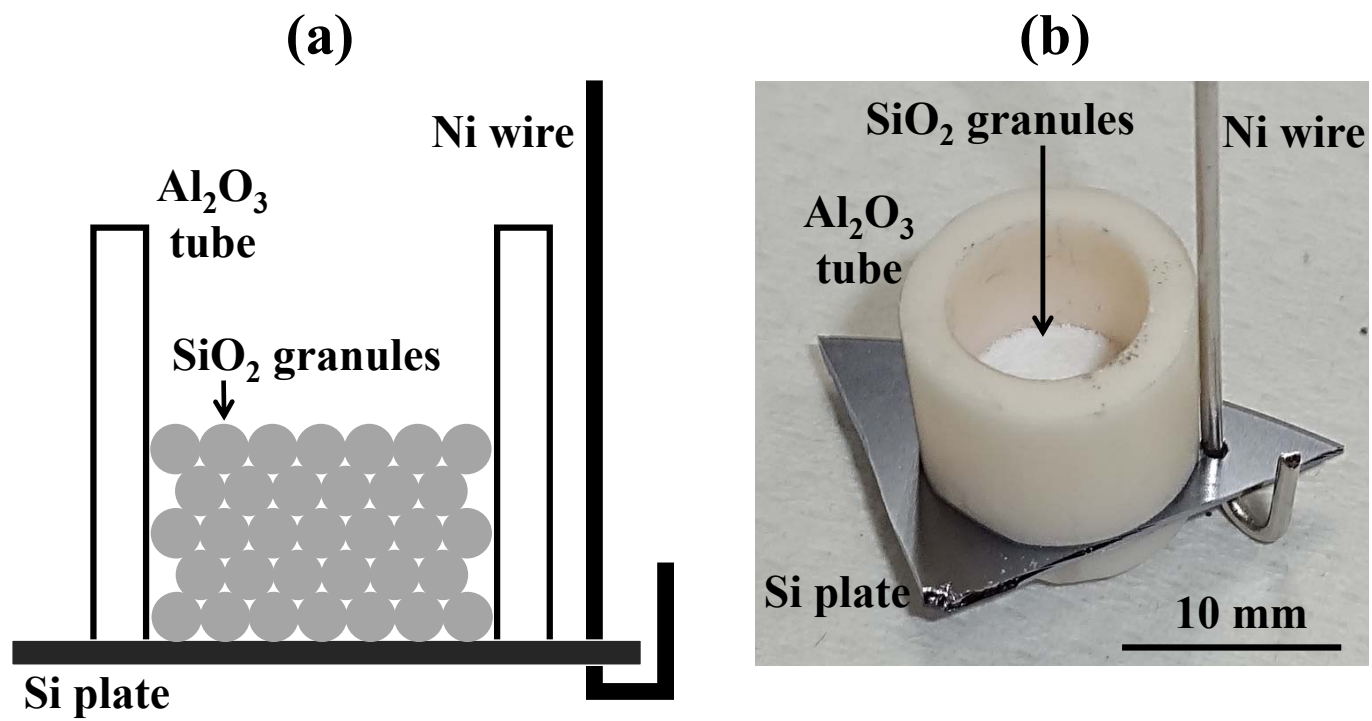


Figure 1. (a) Schematic illustration and (b) photograph of the working electrode.

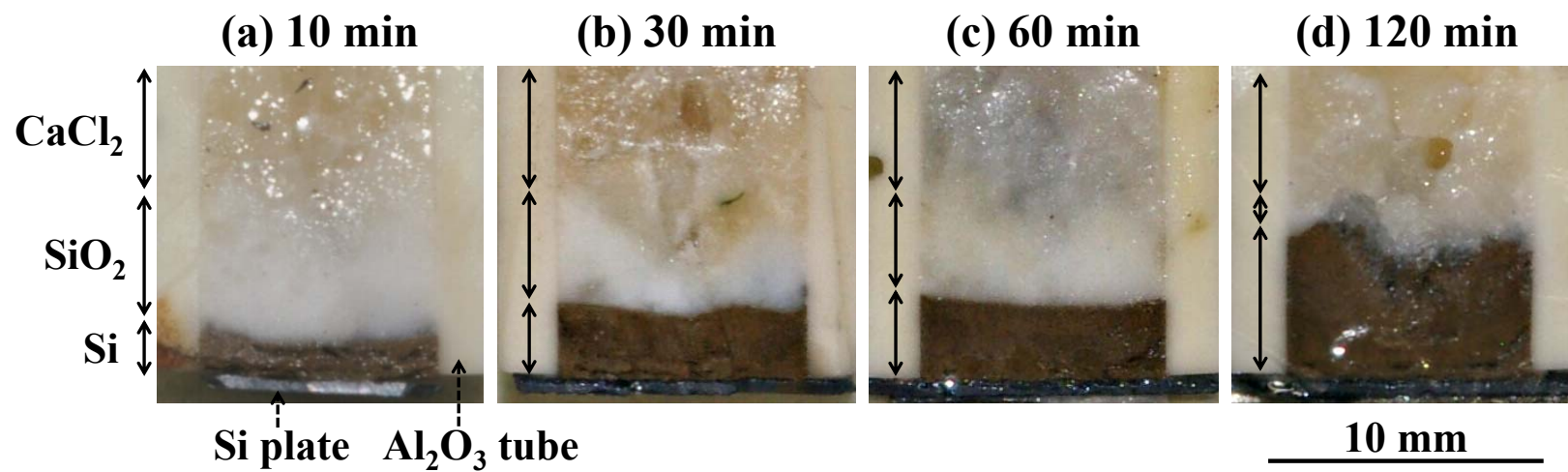


Figure 2. Photographs of the cross sections of working electrodes after electrolysis at 0.5 V vs. Ca²⁺/Ca for 10-120 min in molten CaCl₂ at 1123 K.

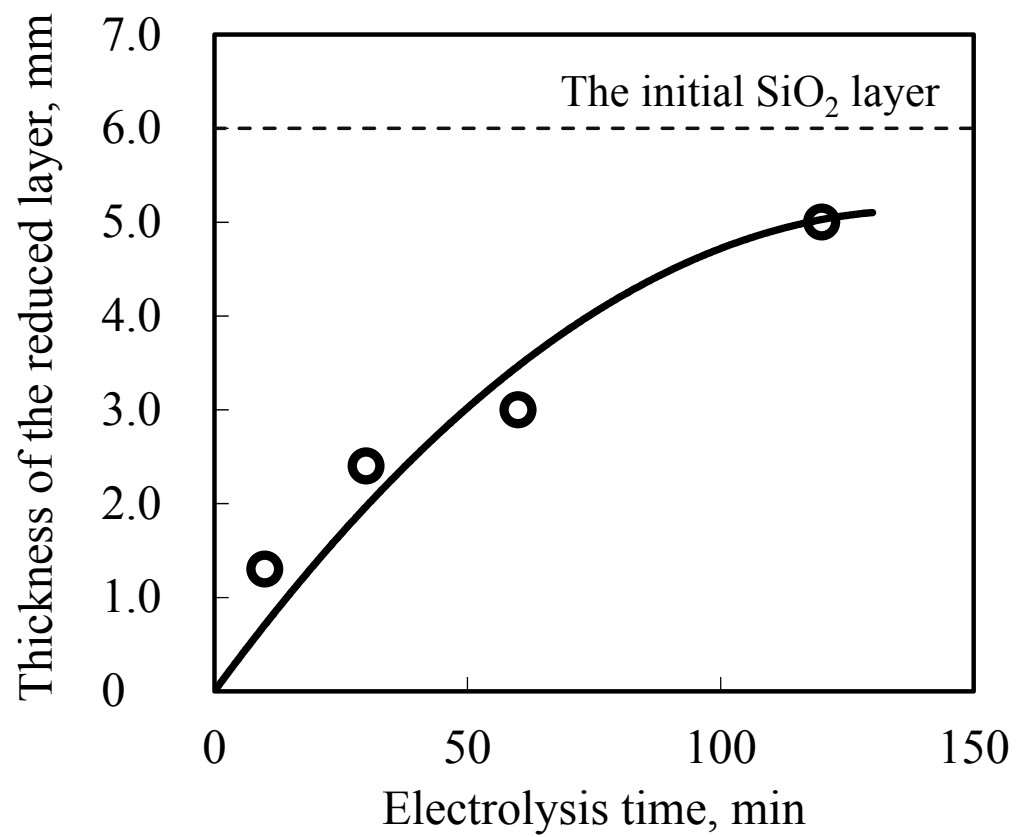


Figure 3. Time dependence of the thickness of the reduced layer of electrochemical reduction of SiO₂ granules by electrolysis at 0.5 V vs. Ca²⁺/Ca for 10-120 min in molten CaCl₂ at 1123 K.

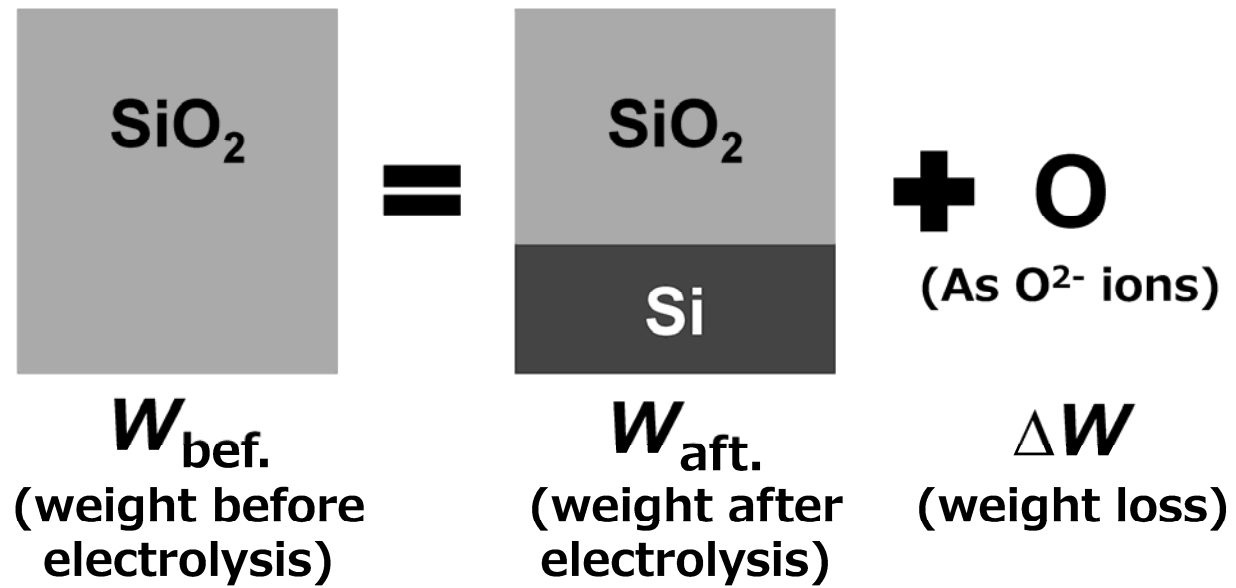


Figure 4. Schematic illustration of mass balance during electrolysis.

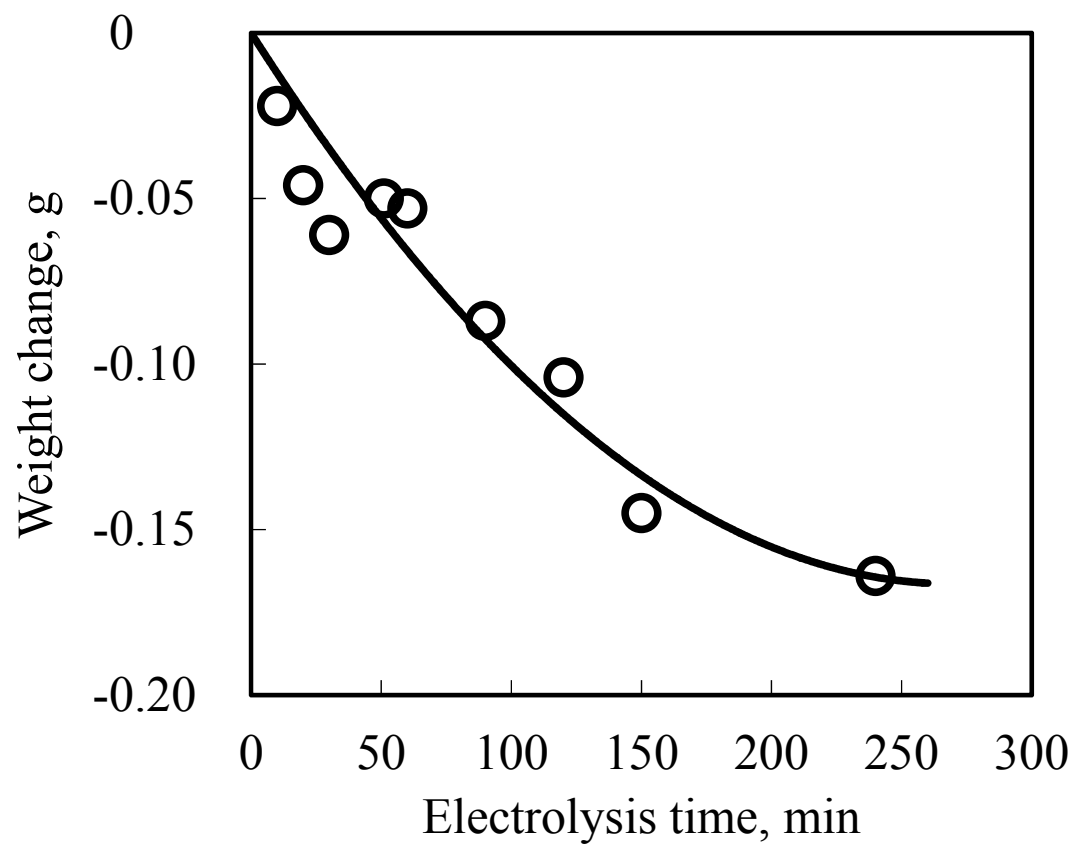


Figure 5. Time dependence of weight change of samples during electrolysis at 0.5 V vs. Ca^{2+}/Ca for 10-240 min in molten CaCl_2 at 1123 K.

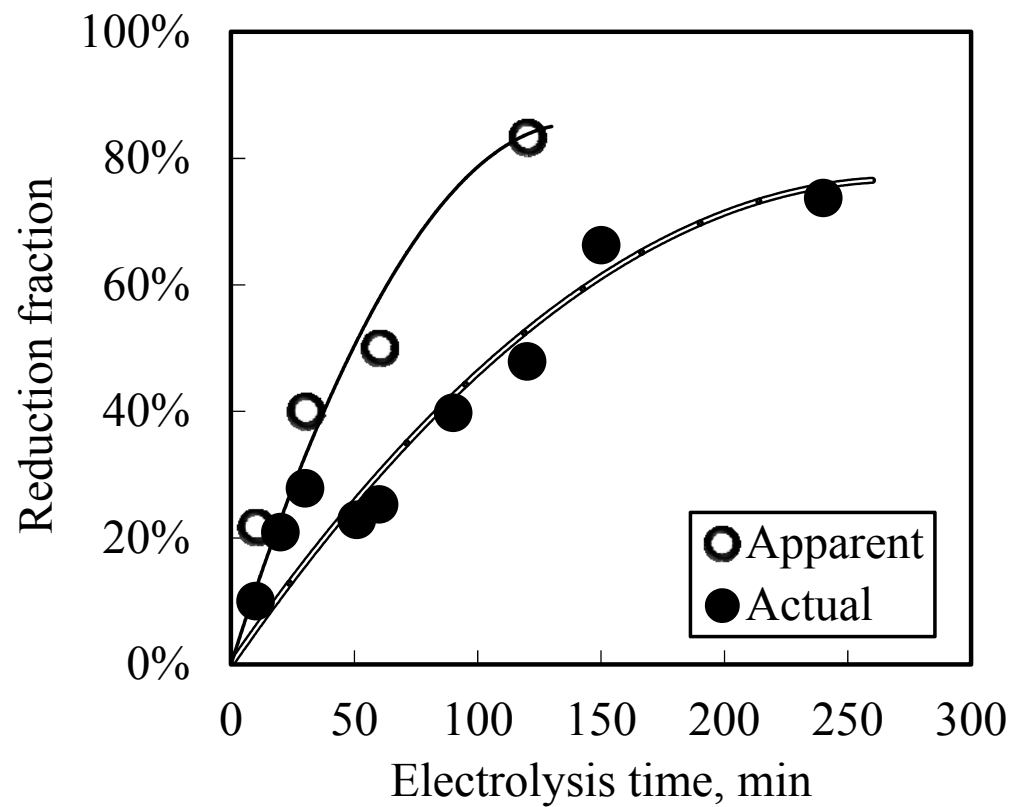


Figure 6. Time dependences of reduction fractions of electrochemical reduction of SiO₂ granules by electrolysis at 0.5 V vs. Ca²⁺/Ca for 10-240 min in molten CaCl₂ at 1123 K.

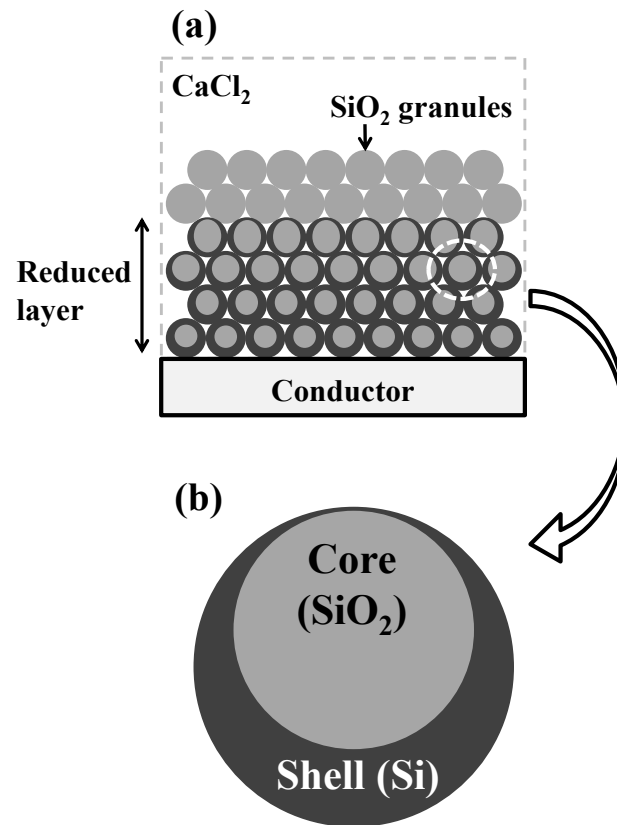


Figure 7. Schematic illustrations of the (a) cross section of the working electrode half way through electrolysis and (b) core (SiO₂)-shell (Si) structure for partly reduced SiO₂ granules.

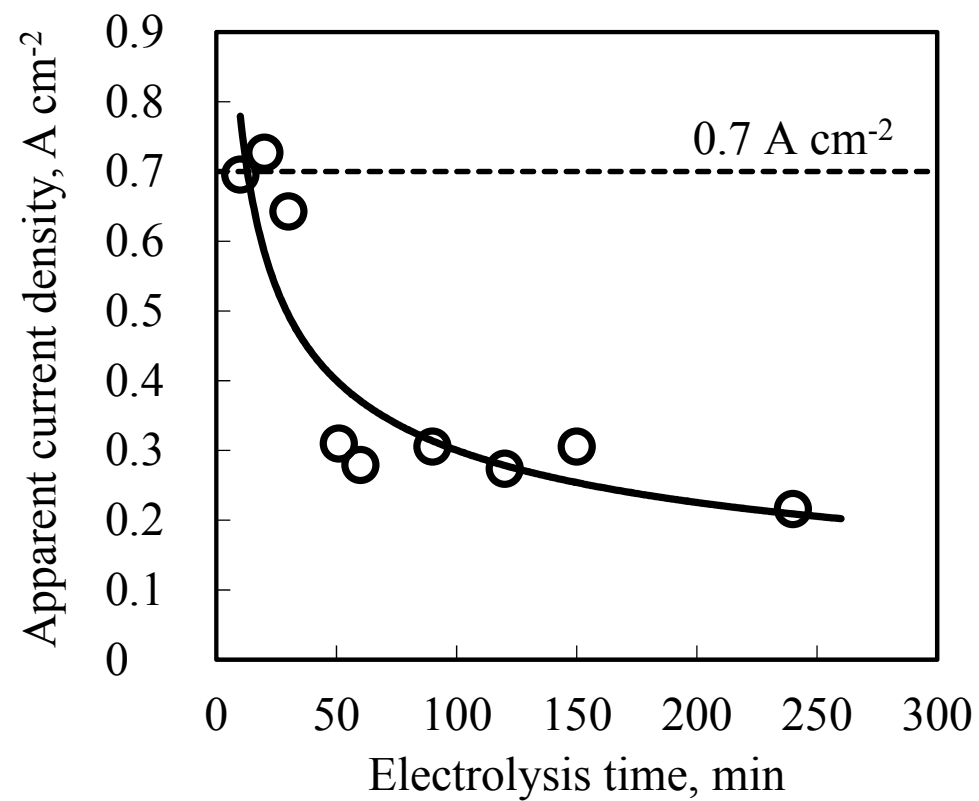


Figure 8. Time dependence of the apparent current density of electrochemical reduction of SiO₂ granules by electrolysis at 0.5 V vs. Ca²⁺/Ca for 10- 240 min in molten CaCl₂ at 1123 K.

Table I. Weight change of samples during electrolysis at 0.5 V vs. Ca^{2+}/Ca for 10-240 min in molten CaCl_2 at 1123 K.

Exp. No.	Time /min	Weight of the sample /g		Weight change /g
		Before electrolysis	After electrolysis	
2-1	10	0.413	0.391	-0.022
2-2	20	0.413	0.367	-0.046
2-3	30	0.411	0.350	-0.061
2-4	50	0.410	0.360	-0.050
2-5	60	0.393	0.340	-0.053
2-6	90	0.410	0.323	-0.087
2-7	120	0.407	0.303	-0.104
2-8	150	0.410	0.265	-0.145
2-9	240	0.417	0.253	-0.164

Table II. Apparent reduction fraction ($F_{app.}$), actual reduction fraction ($F_{act.}$), and apparent current density of direct electrochemical reduction of SiO_2

granules by electrolysis at 0.5 V vs. Ca^{2+}/Ca for 10-240 min in molten CaCl_2 at 1123 K.

Exp. No.	Time /min	$F_{app.}$	$F_{act.}$	Apparent current density / A cm^{-2}
1-1	10	21.7%	-	-
1-2	30	40.0%	-	-
1-3	60	50.0%	-	-
1-4	120	83.3%	-	-
2-1	10	-	10.0%	0.70
2-2	20	-	20.9%	0.73
2-3	30	-	27.8%	0.64
2-4	50	-	22.9%	0.31
2-5	60	-	25.3%	0.28
2-6	90	-	39.8%	0.31
2-7	120	-	47.9%	0.27
2-8	150	-	66.3%	0.31
2-9	240	-	73.7%	0.22